Journal of Alloys and Compounds 591 (2014) 218–223

Contents lists available at ScienceDirect

Journal of Alloys and Compounds

journal homepage: www.elsevier.com/locate/jalcom

Structural, dielectric, ferroelectric and strain properties in $CaZrO_3$-modified $Bi(Mg_{0.5}Ti_{0.5})O_3$–$PbTiO_3$ solid solutions

Wanli Zhao [a], Ruzhong Zuo [a,*], Feng Li [a], Longtu Li [b]

[a] Institute of Electro Ceramics & Devices, School of Materials Science and Engineering, Hefei University of Technology, Hefei 230009, PR China
[b] State Key Laboratory of New Ceramics and Fine Processing, Department of Materials Science and Engineering, Tsinghua University, Beijing 100084, PR China

ARTICLE INFO

Article history:
Received 28 October 2013
Received in revised form 19 December 2013
Accepted 26 December 2013
Available online 7 January 2014

Keywords:
Ceramics
Ferroelectrics
Dielectric properties
Strain properties

ABSTRACT

The structural, dielectric, ferroelectric, strain properties of $(0.89-x)Bi(Mg_{0.5}Ti_{0.5})O_3$–$xPbTiO_3$–$0.11CaZrO_3$ ceramics ($x = 0.45$–0.55) were investigated. A morphotropic phase boundary between rhombohedral relaxor and tetragonal normal ferroelectric phases was identified in the composition range of $0.49 < x < 0.51$. Moreover, a phase transition from ergodic to nonergodic relaxor states was noticed in the composition range of $0.45 < x < 0.51$ with increasing the $PbTiO_3$ content, during which a giant electric field induced strain (~0.32%, $d^*_{33} \sim 640$ pm/V) was observed in the proximity of $x = 0.48$. Such a giant strain is believed to originate from the field induced reversible phase transformation between ergodic relaxor and the long-range ferroelectric phase and this was further confirmed by the measurements of the temperature-dependent ferroelectric polarization/strain loops.

© 2014 Elsevier B.V. All rights reserved.

1. Introduction

Ferroelectric ceramics have long been used in sensors and actuators and have found applications in the fields of aerospace, high technology, and medical instruments [1]. Most of such devices rely on the piezoelectric properties of the material to achieve the high bandwidth and linear actuation. However, the strain available in this class of materials is limited around 0.1% which would not be compatible for some applications where a large strain is valued. Therefore, $PbZrO_3$ (PZ)-based antiferroelectric (AFE) materials attracted much attention due to its large strain value (volume effect) which originates from an electric field induced AFE-ferroelectric (FE) phase transition [2,3]. This phase transition manifests itself by the apparent double-hysteresis loops.

In addition to the Pb-based materials, Bi-based perovskite-structured solid solutions of $BiMeO_3$–$PbTiO_3$ (PT) (*Me* = Mg, Ti, Fe, etc.,) have also attracted lots of attention in recent years. Some of these Bi-based systems have also been reported to exhibit a giant strain through the modification of a slight amount of second phases [4–7]. $Bi(Mg_{0.5}Ti_{0.5})O_3$ (BMT)-based system was reported to exhibit a large strain value (up to ~0.4%, comparable to that observed in AFE materials) under high external electric fields through the substitution of some zirconates [4–6]. Initially, this large strain value was ascribed to a field-forced phase transition from AFE to FE, which was only manifested by the pinched polarization vs. electric field loops (*P*–*E*) [4,5]. Later on, the achievement of the giant strain was considered to stem from a change in the dynamics of the polar nanoregions (PNRs) [6].

However, it is of importance to note that, despite of the different explanations for the generation of giant strains, the achievement of a large strain in these BMT-based systems was usually accompanied by the evolution of the dielectric property from a ferroelectric state to a relaxor state [4,6]. Interestingly, it has been recently found that the ferroelectric to relaxor phase transition could occur when the tolerance factor (t) decreased by doping [8,9]. The tolerance factor was proposed by Goldschmidt [10], which is an indicator for the stability and distortion of ABO_3 perovskite structure, and expressed as $t = (R_A + R_O)/\sqrt{2}(R_B + R_O)$, where R_A, R_B and R_O are the ionic radii of *A*- and *B*-site cations and oxygen, respectively. It is clear that the decrease in tolerance factor is mathematically related with the substitution of smaller ions on *A*-sites and/or larger ions on *B*-sites.

Based on the above discussions, $CaZrO_3$ (CZ) was selected as a new modifier in this study for its smaller ions on *A*-sites ($CN = 12$, $R_{Ca} = 1.34$ Å < $R_{Bi} = 1.45$ Å < $R_{Pb} = 1.49$ Å) and larger ions on *B*-sites ($CN = 6$, $R_{Zr} = 0.72$ Å, $R_{Mg} = 0.72$ Å > $R_{Ti} = 0.605$ Å) [11]. The ionic radius of Bi^{3+} ($CN = 12$) used here was not estimated by using a linear extrapolation method [12]. Furthermore, if compared with the previous study [4–6], it is easy to note that the ionic radii of Ca^{2+} is also smaller than Ba^{2+} and Pb^{2+} ($CN = 12$, $R_{Ca} = 1.34$ Å < $R_{Pb} = 1.49$ Å < $R_{Ba} = 1.61$ Å). Thus, CZ was considered as a more appropriate one to modify the BMT–PT system than other zirconates because it may more obviously decrease the tolerance factor of the system. Therefore, the addition of a certain amount of CZ into the BMT–PT system was expected to induce a dielectric

* Corresponding author. Tel./fax: +86 551 62905285.
E-mail address: piezolab@hfut.edu.cn (R. Zuo).

0925-8388/$ - see front matter © 2014 Elsevier B.V. All rights reserved.
http://dx.doi.org/10.1016/j.jallcom.2013.12.229

relaxor behavior from the merely diffuse-typed BMT–PT system [13]. The purpose of this study was aimed at the evolution of the structural and electrical properties of 11 mol% CZ modified BMT–PT compositions ((0.89 − x)BMT–xPT–0.11CZ) with the change of BMT and PT contents. The influence of the variation of the CZ content will be systematically explored elsewhere. It is believed that the Curie temperature of the system would be too low (possibly lower than room temperature) if the CZ content is too high. A giant strain of ~0.32% (d^*_{33} ~ 640 pm/V) was achieved in the x = 0.48 composition under an electric field of 5 kV/mm. The origin of this large strain value was further explained by a couple of measurements such as dielectric-temperature-frequency spectrum, ferroelectric polarization/strain hysteresis loops as well as the polarization current density loops.

2. Experimental

The (0.89 − x)Bi($Mg_{0.5}Ti_{0.5}$)O_3–xPbTiO_3–0.11CaZrO_3 (x = 0.45–0.55, BMT–xPT–CZ) ceramics were prepared by a conventional solid-state reaction method using high-purity (>99%) Bi_2O_3, TiO_2, PbO, ZrO_2, $CaCO_3$ and $(MgCO_3)_4{\cdot}Mg(OH)_2{\cdot}5H_2O$ as raw-materials. The starting powders were weighed according to the stoichiometric formula and ball-milled for 6 h in ethanol with zirconia balls. The dried powders were calcined twice at 900 °C for 2 h and then ball milled again for 8 h. The powders were pressed into pellets with 10 mm in diameter and the pellets were sintered in sealed crucibles at 1150 °C for 2 h.

The crystal structure was examined by an X-ray diffractometer (XRD, D/Max-RB, Rigaku, Tokyo, Japan) using Cu Kα radiation. For electrical measurements, the silver paste was painted on major sides of the samples and fired at 550 °C for 30 min. The samples were poled at a dc field of 5 kV/mm at room temperature for 5 min in silicone oil. The small-signal piezoelectric constant d_{33} was measured by using a Belincourt meter (YE2730A, Sinocera, Yangzhou, China). Dielectric properties were measured as a function of temperature and frequency by an LCR meter (Agilent E4980A, Santa Clara, CA) in the frequency range of 1 kHz–1 MHz in the temperature range 25–500 °C. The P–E loops and electric field-induced strain (S–E) curves as a function of composition and temperature were measured by using a ferroelectric measuring system (Precision multiferroelectric, Radiant Technologies Inc., Albuquerque, NM) with an accessory laser interferometer vibrometer (AE SP-S 120E, SIOS Meβtechnik, GmbH, Ilmenau, Germany).

3. Results and discussion

Fig. 1 shows the XRD patterns of the BMT–xPT–CZ ceramics. The results revealed a single perovskite structure without any apparent secondary phases for all the studied compositions, as shown in Fig. 1(a). Detailed XRD scan of the (111) peak is shown in Fig. 1(b). It is obvious from Fig. 1(b) that a discontinuous variation of the (111) diffraction peak was observed between x = 0.49 and x = 0.51. For samples with x < 0.49, the (111) diffraction peak shifted to higher diffraction angles with increasing the PT content while the peak jumped to the lower diffraction angles abruptly when x reaches 0.51. This discontinuous change of the diffraction peak positions is usually related to a change of the phase structure [14]. To further confirm this phase transition, the change tendency of the (200) diffraction lines are given in Fig. 1(c). It is clear that samples with x < 0.49 have a rhombohedral structure as evidenced by the single $(200)_R$ diffraction lines while samples with x > 0.51 have a tetragonal structure as evidenced by the peak splitting of $(002)_T$ and $(200)_T$ diffraction lines. Therefore, a morphotropic phase boundary (MPB) between tetragonal and rhombohedral phases can be identified between x = 0.49 and x = 0.51. Moreover, it can be seen from Fig. 1(c) that there existed a gradual shift of the $(200)_R$ diffraction peak towards higher angles with increasing the PT content. This is probably due to the relatively small ionic radius of Ti^{4+} compared with that of Mg^{2+} at the B-site (CN = 6, R_{Ti} = 0.605 Å < R_{Mg} = 0.72 Å) although the A-site ionic radius of Pb^{2+} (CN = 12, R_{Pb} = 1.49 Å) is slightly bigger than that of Bi^{3+} (CN = 12, R_{Bi} = 1.45 Å) [11,12]. On the other hand, one can clearly see that the $(002)_T$ and $(200)_T$ diffraction peaks appeared and simultaneously the tetragonality gradually increased from 1.017 for the x = 0.49 sample to 1.030 for the x = 0.55 sample as the composition is across the MPB zone into the tetragonal phase zone.

The dielectric permittivity measured as functions of temperature and frequency for both unpoled and poled samples is shown in Fig. 2. Typical relaxor behavior could be observed near the temperatures for the dielectric maximum (T_m) for all samples, as shown in Fig. 2. Besides, it is clear that the samples with x > 0.51 (tetragonal phase) possessed a spontaneous ferroelectric to relaxor phase transition with increasing the temperature and a transition temperature $T_{f,r}$ was observed, as shown in Fig. 2(g) and (h). It is believed that the relaxor behavior should originate from the dielectric behavior evolution of the BMT–PT system through the modification of 11 mol% $CaZrO_3$. The BMT-PT system was reported to own a diffuse phase transition behavior around T_m in the absence of frequency dispersion [13]. Due to a decrease of the tolerance factor after the substitution of BMT-PT with 11 mol% $CaZrO_3$, the dielectric relaxation behavior could be expected to occur in this system as discussed previously [8,9]. Generally speaking, the size and dynamics of the polar nanoregions (PNRs) were believed to play an important role in relaxor behavior and the size and dynamics of the PNRs were determined by the local random field which was formed due to the disordered distribution of different ions at

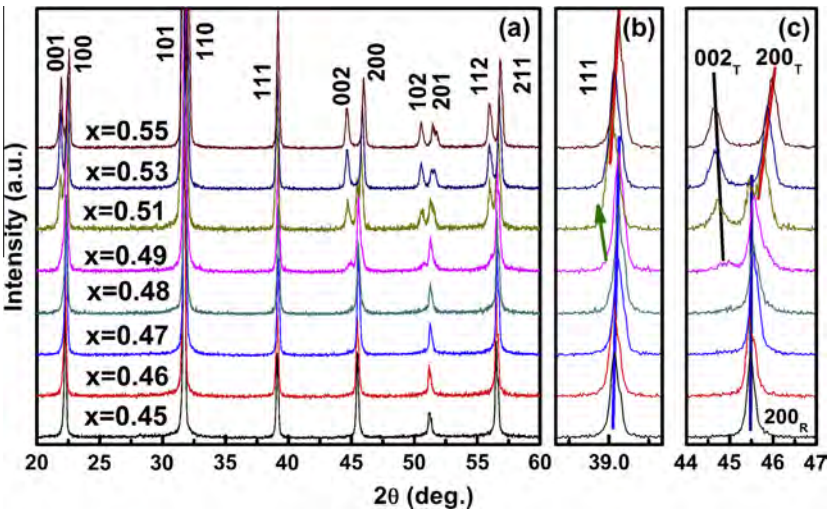

Fig. 1. Powder XRD patterns of BMT–xPT–CZ ceramics as a function of the PT content, (b) locally magnified (111) diffraction peaks and (c) locally magnified (200) diffraction peaks.

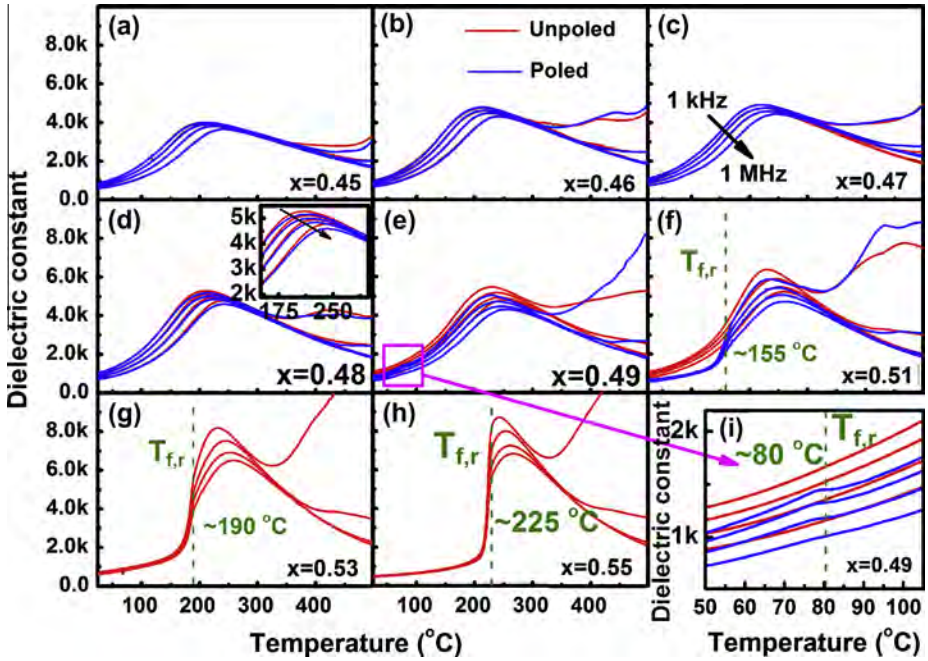

Fig. 2. Dielectric permittivity as functions of temperature and frequency for poled and unpoled BMT–*x*PT–CZ ceramics with (a) $x = 0.45$, (b) $x = 0.46$, (c) $x = 0.47$, (d) $x = 0.48$, (e) $x = 0.49$ and (f) $x = 0.51$, and only for unpoled BMT–*x*PT–CZ samples with (g) $x = 0.53$ and (h) $x = 0.55$; (i) the locally magnified curves in Fig. 2(e) in a relatively low temperature range.

one or more equivalent crystallographic sites of the structure [6,15–17]. It has been demonstrated that local random field, existing in BMT–PT system, is not strong enough to break the long-range order [6]. The introduction of CZ could make the local random fields become strong enough to disrupt the long-range order. As a result, large domains in BMT–PT tend to become smaller and the correlation of each domain becomes weaker, such that they can exhibit a dynamic behavior, leading to the frequency dependence of the dielectric constant. For samples with higher PT contents ($x > 0.51$), the appearance of normal ferroelectric state would be considered as a result of the large tetragonality which would prevent the formation of PNRs at room temperature. However, samples with $x < 0.49$ would exist in an ergodic relaxor state or a nonergodic relaxor state with an average rhombohedral symmetry at room temperature. For compositions with $0.49 < x < 0.51$ (MPB), the samples should be a mixture of rhombohedral relaxor and tetragonal normal ferroelectric.

For relaxor ferroelectrics, it was generally believed that the PNRs would exist in a randomly distributed state at temperatures a few hundred degrees above the Curie temperature [18], the average size of PNRs would increase and their dynamics slows down with decreasing the temperature, such that at an extremely low temperature an ergodic relaxor either spontaneously transforms into long-range ordered ferroelectrics with micron-sized domains at $T_{f,r}$ [19], or can be simply frozen into a nonergodic relaxor with a short-range polar order at a critical freezing temperature T_f [20]. On the other hand, it is known that the application of a strong enough electric field could overcome the random fields and induce a macroscopically detectable ferroelectric order while the induced ferroelectric order can be either unstable or stable on removal of the applied electric field depending on whether the relaxor is an ergodic state or nonergodic state at room temperature [21,22]. Then, the different dielectric behavior before and after poling for all the six studied compositions could be explained as follows. As can be seen from Fig. 2(f), an obvious difference was observed in the $x = 0.51$ samples before and after poling. The poled $x = 0.51$ sample exhibits a normal dielectric behavior at low temperature range but a typical relaxor behavior around T_m, which is similar to that of the unpoled samples with a tetragonal phase (such as $x = 0.53$). This indicates that the PNRs in the $x = 0.51$ sample could be irreversibly transformed into a long-range order by a strong enough external electric field. Upon heating, the induced long-range order breaks down into short-range ones again at a critical temperature ($T_{f,r} \sim 155$ °C). Therefore, the rhombohedral relaxor ferroelectric in $x = 0.51$ sample should be believed to exist in a nonergodic state. On the other hand, it could be detected from Fig. 2(e) (more clearly shown in Fig 2(i)) that a dielectric anomaly ($T_{f,r} \sim 80$ °C) occurred in the dielectric permittivity curves for the poled sample with $x = 0.49$. In addition, a weak frequency dependence of the dielectric permittivity could be still observed in this composition after poling, which may indicate that some of the rhombohedral relaxor phases in $x = 0.49$ sample would exist in an ergodic state while others existed in a nonergodic state. Such a phenomenon further suggests that the $x = 0.49$ composition might have a T_f value slightly higher than room temperature. In contrast, no obvious distinction before and after poling could be detected for $x = 0.48$ sample, meaning that this sample was classified as an ergodic relaxor at room temperature. It is noted that any field-induced change in ergodic relaxors would revert to its original state on removal of electric field [22]. However, a careful comparison of the two states for the $x = 0.48$ sample revealed that the electric poling process actually induces a depression in the spectra at the dielectric maximum, as shown in inset of Fig. 2(d). This implies that the poling treatment at room temperature does induce an irreversible change. Hence, $x = 0.48$ sample is considered as a mixture of ergodic and nonergodic relaxor at room temperature but is dominated by the ergodic relaxor state. On the other hand, no any difference can be detected between the poled and unpoled samples with $x < 0.48$, as can be seen from Fig. 2(a)–(c). Thus, all the three samples existed in an ergodic state at room temperature and the T_f values for these three samples should be lower than room temperature. Based on the above discussion, a conclusion

could be drawn that the freezing temperature T_f rapidly decreased from temperature higher than room temperature for samples with higher PT contents to below room temperature for samples with $x < 0.48$. As a result, all compositions with $x < 0.48$ exhibited no difference in the dielectric response before and after poling at room temperature.

Fig. 3 depicts the room-temperature P–E loops as well as the corresponding current density loops (J–E). It is obvious that a saturated and square P–E loop was observed for the sample with $x = 0.49$ together with a single sharp polarization current peak, both of which are typical for materials with a long-range ferroelectric order. On the contrary, slim and unsaturated P–E loops were obtained for samples with $x = 0.45$ and 0.47 with relatively low remanent polarization (P_r) values while no any obvious current peaks could be observed but only a broad and flat current platform was formed. All these features are typical for ergodic relaxors. In contrast, slightly pinched P–E loops were observed for the composition with $x = 0.48$, simultaneously an additional current peak was clearly observed. It was demonstrated that the coexistence of ergodic and nonergodic relaxors would be responsible for the presence of the two current peaks [23]. Here, it should be noted that even though the coexistence of ergodic and nonergodic relaxors was also observed in the $x = 0.49$ sample, yet only a single sharp polarization current peak was obtained rather than two current peaks. This may indicate that the amount of the ergodic phase in this composition would be very low, such that it would have no obvious influence on the ferroelectric property. For samples with higher PT contents ($x \geqslant 0.51$), accompanied by the increase of the tetragonality, the coercive field (E_c) experienced an obvious increase. As a result, the applied field strength is not strong enough to induce a full poling state for these samples so that the values of the maximum polarization and remanent polarization decreased drastically.

Fig. 4(a) and (b) shows the electric field induced S–E curves measured at a frequency of 1 Hz as functions of bipolar and unipolar electric fields at room temperature. The evolution of the positive strain (S_{pos}, see Fig. 4(a)) and negative strain (S_{neg}, see Fig. 4(a)) with increasing the PT content is summarized in Fig. 4(c). At the same time, the change tendency of the corresponding small-signal d_{33} is also shown in Fig. 4(c). It is obvious that a nearly linear unipolar strain behavior with a relatively low hysteresis was observed for the $x = 0.49$ sample. Meanwhile, a notable S_{neg} value was obtained in this sample during the bipolar measurement. This is a typical feature for ferroelectric materials with long-range ferroelectric order. This result is consistent with the previous analysis on the P–E measurement (Fig. 3). Similar results were also obtained for samples with higher PT contents ($x > 0.49$) as shown in Fig. 4(a) and (b), indicating the long-range ferroelectric nature for these compositions. For samples with lower PT contents ($x < 0.49$), the S_{neg} value nearly vanished (the vanishing of the S_{neg} value was considered as a strong evidence of the disappearance of

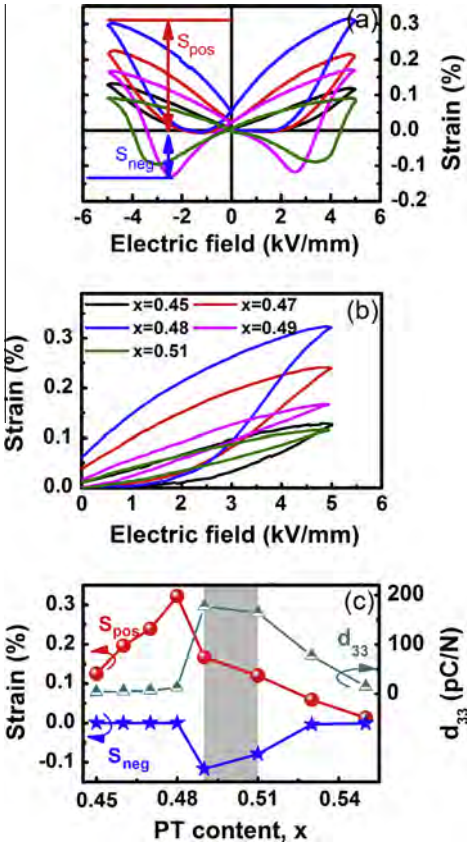

Fig. 4. (a) Bipolar and (b) unipolar S–E curves measured at 1 Hz at room temperature for BMT–xPT–CZ ceramics, and (c) the variation of both S_{pos} and S_{neg} as well as the small-signal d_{33} values with the PT content.

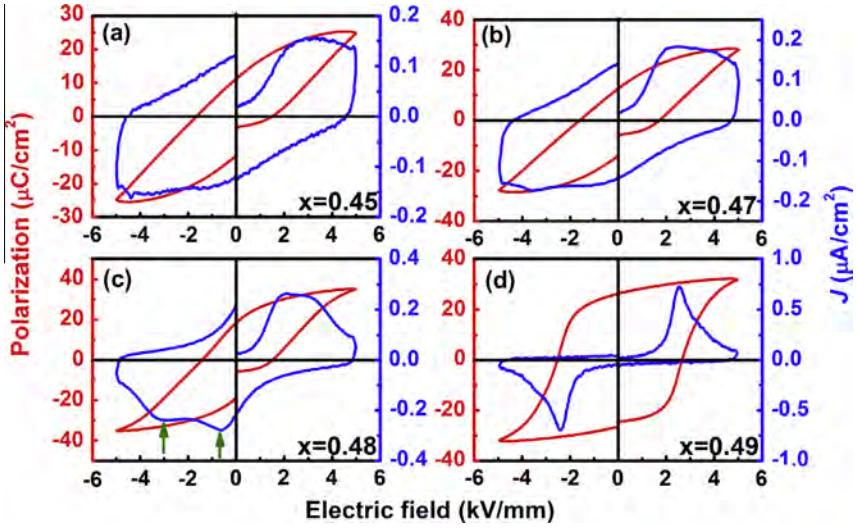

Fig. 3. P–E hysteresis loops and associated J–E curves measured at a frequency of 1 Hz for BMT–xPT–CZ ceramics: (a) $x = 0.45$, (b) $x = 0.47$, (c) $x = 0.48$ and (d) $x = 0.49$.

the long-range ferroelectric order) and all the samples show sprout-shaped bipolar strain loops and *S*-shaped unipolar strain curves with pronounced hysteresis. All the features are typical for ergodic relaxors. At the same time, a near-zero small-signal d_{33} could be detected for samples with $x < 0.49$. This could also confirm the ergodic state for samples with low PT contents. Moreover, a large strain of ~0.32% ($d^*_{33} \sim 640$ pm/V) was obtained for the sample with $x = 0.48$ which was believed to lie around the boundary between ergodic and nonergodic relaxor as discussed above. It was demonstrated that, owing to the two-phase coexistence, the free energy of the field induced long-range ferroelectric order in this composition appears so competitive with that of the ergodic phase at zero electric field, that the long-range ferroelectric order can be easily induced by an external electric field [24]. This field induced reversible ergodic relaxor-ferroelectric phase transition was considered to be responsible for the observed field induced giant strain. Simultaneously, it is apparent from Fig. 4(c) that the achievement of the electric field induced large strain was accompanied by a drastic decrease in the S_{neg} value and similar phenomena have also been observed in other Bi-containing perovskite-structured ferroelectrics [6,24]. As for the piezoelectric property of this system, it could be seen from Fig. 4(c) that a peak d_{33} value (~175 pC/N) was obtained around the MPB region, which is similar to that observed in conventional Pb-based piezoelectric ceramics.

To further confirm the exact contribution of the phase transition to the obtained giant strain value in this study, the temperature dependent *P*–*E* loops as well as the bipolar *S*–*E* curves for the $x = 0.49$ sample were collected, as shown in Fig. 5. It is obvious that a continued decrease of E_c as well as the P_r value was observed with increasing the temperature as shown in Fig. 5(a). A pinched *P*–*E* loop, which is similar to that of the sample with $x = 0.48$, was obtained at 80 °C and a slim loop was obtained at 100 °C, showing an obvious feature of ergodic relaxors. The result indicated that the property of this sample gradually transformed to a pure ergodic state with increasing temperature. On the other hand, it could be seen that the maximum polarization values were comparable in the whole measuring temperature range, indicating that long-range ferroelectric order could be obtained under the application of a strong enough external field (e.g. 5 kV/mm in this study). However, as the material gradually transformed into the ergodic state with increasing the measuring temperature, the induced long-range ferroelectric order could no longer be maintained after removal of the electric field, resulting in a reduction of the P_r. At the same time, the measured bipolar *S*–*E* curves (Fig. 5(b)) also exhibited a change from butterfly shape to sprout shape with increasing the measuring temperature. The value of S_{neg}, which is obvious at room temperature, showed a tendency of decrease and totally disappeared at 80 °C just where a maximum strain (~0.32%, $d^*_{33} \sim 640$ pm/V) was obtained. Thus, the state of this sample at 80 °C could be considered as a critical point (T_f) between ergodic and nonergodic and this result further confirmed the contribution of the phase transition between ergodic relaxor and the long-range ferroelectric phase to the obtained giant strain value in this study.

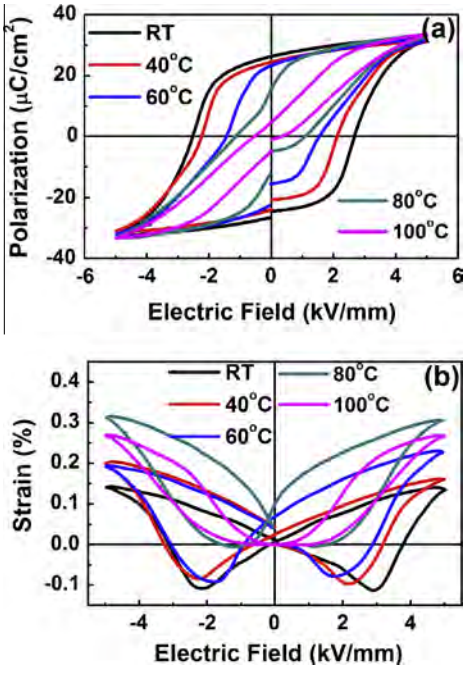

Fig. 5. (a) *P*–*E* hysteresis loops and (b) bipolar *S*–*E* curves of BMT–0.49PT–CZ ceramic with varying temperature from room temperature (RT) to 100 °C at 1 Hz.

4. Conclusions

The $(0.89 - x)Bi(Mg_{0.5}Ti_{0.5})O_3$–$xPbTiO_3$–$0.11CaZrO_3$ solid solution ceramic were investigated in terms of their structure, dielectric behavior and electric-field induced strain characteristics. An MPB between rhombohedral relaxor and tetragonal normal ferroelectric phases was identified in the composition range between $x = 0.49$ and $x = 0.51$. The dielectric property of this system was found to gradually transform from an ergodic relaxor to a nonergodic relaxor in the composition range of $0.45 < x < 0.51$ with increasing the PT content, during which a giant electric field induced strain (~0.32%, $d^*_{33} \sim 640$ pm/V) was observed around the boundary ($x = 0.48$) between ergodic and nonergodic relaxors. The origin of this giant strain was believed to be related with the electric field induced phase transition between ergodic relaxor and the long-range ferroelectric phase.

Acknowledgements

Financial support from the National Natural Science Foundation of China (Grant Nos. 51272060, 51332002), the Natural Science Foundation Anhui Province (Grant No. 1108085J14) and an opening fund of State Key Laboratory of New Ceramic and Fine Processing at Tsinghua University is gratefully acknowledged.

References

[1] L.E. Cross, Mater. Chem. Phys. 43 (1996) 108–115.
[2] W.Y. Pan, Q.M. Zhang, A. Bhalla, L.E. Cross, J. Am. Ceram. Soc. 72 (1989) 571–578.
[3] K. Markowski, S.E. Park, S. Yoshikawa, L.E. Cross, J. Am. Ceram. Soc. 79 (1996) 3297–3304.
[4] L.L. Fan, J. Chen, H.J. Kang, L.J. Liu, L. Fang, J.X. Deng, R.B. Yu, X.R. Xing, J. Appl. Phys. 111 (2012) 104118.
[5] J. Chen, J.Y. Li, L.L. Fan, N. Zou, P.F. Ji, L.J. Liu, L. Fang, H.J. Kang, X.R. Xing, J. Appl. Phys. 112 (2012) 074101.
[6] J. Fu, R.Z. Zuo, Acta Mater. 61 (2013) 3687–3694.
[7] L.L. Fan, J. Chen, S. Li, H.J. Kang, L.J. Liu, L. Fang, X.R. Xing, Appl. Phys. Lett. 102 (2013) 022905.
[8] V.Q. Nguyen, H.S. Han, K.J. Kim, D.D. Dang, K.K. Ahn, J.S. Lee, J. Alloys Comp. 511 (2012) 237–241.
[9] I.K. Hong, H.S. Han, C.H. Yoon, H.N. Ji, W.P. Tai, J.S. Lee, J. Intell. Mater. Syst. Struct. 24 (2013) 1343–1349.
[10] V.M. Goldschmidt, Naturwissenschaften 14 (1926) 477–485.
[11] R.D. Shannon, Acta Cryst. A32 (1976) 751–767.
[12] A. Tkach, A. Almeida, J.A. Moreira, T.M. Correia, M.R. Chaves, O. Okhay, P.M. Vilarinho, I. Gregora, J. Petzelt, J. Appl. Phys. 98 (2011) 052903.
[13] C.A. Randall, R. Eitel, B. Jones, T.R. Shrout, D.I. Woodward, I.M. Reaney, J. Appl. Phys. 95 (2004) 3633–3639.
[14] W.W. Zuo, R.Z. Zuo, W.L. Zhao, Ceram. Int. 39 (2013) 725–730.
[15] V. Westphal, W. Kleemann, M.D. Glinchuk, Phys. Rev. Lett. 68 (1992) 847–850.
[16] Y. Liu, R.L. Withers, B. Nguyen, K. Elliott, Appl. Phys. Lett. 91 (2007) 152907.
[17] V.V. Shvartsman, D.C. Lupascu, J. Am. Ceram. Soc. 95 (2012) 1–26.

[18] L. Xie, Y.L. Li, R. Yu, Z.Y. Cheng, X.Y. Wei, X. Yao, C.L. Jia, K. Urban, A.A. Bokov, Z.G. Ye, J. Zhu, Phys. Rev. B 85 (2012) 014118.
[19] F. Chu, I.M. Reaney, N. Setter, J. Appl. Phys. 77 (1995) 1671–1676.
[20] V. Bobnar, Z. Kutnjak, R. Pirc, R. Blinc, A. Levstik, Phys. Rev. Lett. 84 (2000) 5892–5895.
[21] J.F. Li, X.H. Dai, A. Chow, D. Viehland, J. Mater. Res. 10 (1995) 926–938.
[22] V. Bobnar, Z. Kutnjak, R. Pirc, A. Levstik, Phys. Rev. B 60 (1999) 6420–6427.
[23] G. Viola, H.P. Ning, X.J. Wei, M. Deluca, A. Adomkevicius, J. Khaliq, M.J. Reece, H.X. Yan, J. Appl. Phys. 114 (2013) 014107.
[24] W. Jo, T. Granzow, E. Aulbach, J. Rödel, D. Damjanovic, J. Appl. Phys. 105 (2009) 094102.